

A method for measuring the quality parameters of image intensifier based on projecting phase-shifting gratings

SONG SUN, YIPING CAO*, CHENG CHEN, GUANGKAI FU, YAPIN WANG, XINGFEN XU

Opto-Electronics Department, Sichuan University, Chengdu, 610064, China

*Corresponding author: ypcao@scu.edu.cn

A method for measuring the quality parameters of image intensifier based on projecting phase-shifting gratings is proposed. A set of designed phase-shifting gratings are projected into the measuring system orderly to obtain the magnification parameter of the measured image intensifier, and the phase caused by the measured image intensifier. After obtaining the referential phase caused by only the magnification of the measured image intensifier, the phase caused by the distortion of the measured image intensifier is extracted by phase calculating and phase unwrapping. Both the global distortion and the partial distortion of the measured image intensifier can be measured by phase-to-distortion matching at the same time. The experimental results show that the proposed method can measure the multiple quality parameters of image intensifier effectively.

Keywords: phase measurement, phase-shifting grating, distortion, image intensifier, imaging quality parameter.

1. Introduction

The image intensifier [1–5] is the core component of night-vision devices. It has been applied in different fields, such as national defense [6] or space exploration [7]. The image intensifier with excellent imaging performance is the basic requirement in industrial manufacture. Generally, it refers to the quality parameters of image intensifier including magnification and distortion [8, 9]. McROBBIE and NIETO-CAMERO researched the performance of image intensifier by using the modulation transfer function (MTF) [10]. CUELENAERE adopted the principle of optical lens to study the quality parameters of image intensifier [11].

Up to now, most methods for researching the quality parameters or performance of image intensifier have a common problem that the cost of time is too high, so the measuring efficiency needs to be improved. The multi-parameter measuring method of image intensifier based on Fourier transform phase measurement (FTPM) has been proposed [12]. It ameliorates the measuring efficiency because the multiple quality parameters of image intensifier can be obtained at the same time. Unfortunately, the ef-

fective signal is likely to be damaged due to the filtering operation [13–16]. Specially, the high frequency components caused by the partial distortion of the measured image intensifier are smoothed during the filtering, which influences the measuring result.

The phase measurement profilometry (PMP) has been proposed by SRINIVASAN *et al.* since 1984 [17]. The measuring accuracy of phase measurement with PMP is better than that with other methods for there is no filtering or damaged information. Here, a method for measuring the quality parameters of image intensifier based on projecting phase-shifting gratings (PPSG) is proposed. A set of phase-shifting gratings [18–21] are projected into the measuring system orderly to obtain the magnification parameter of the measured image intensifier, and the phase caused by the measured image intensifier. After the magnification parameter of the measured image intensifier is obtained, another set of phase-shifting gratings which purposely remove the impact of the magnification parameter of the measured image intensifier are projected into the measuring system one by one to obtain the referential phase caused by only the magnification of the measured image intensifier. The phase caused by the distortion of the measured image intensifier is extracted by phase calculating and phase unwrapping [22]. Both the global distortion and the partial distortion of the measured image intensifier can be obtained by the phase-to-distortion matching at the same time. The proposed method provides a theoretical basis or technical support for measuring the quality parameters of image intensifier. The measured results can be fed back to the manufacturer for calibrating the measured quality parameters of image intensifier, which can promote the manufacturing technique of image intensifier.

2. Image intensifier system

2.1. Organization structure of image intensifier system

The structure chart of image intensifier system is as shown in Fig. 1. It contains five components that are objective lens, photocathode, electron lens, phosphor screen and eyepiece. Because of the photoelectric effect, abundant electrons gush out from the photocathode while a beam of external light is received by the objective lens, and these electrons are enhanced by the electron lens. The enhanced electrons are transmitted onto the phosphor screen and the image can be observed with the eyepiece.

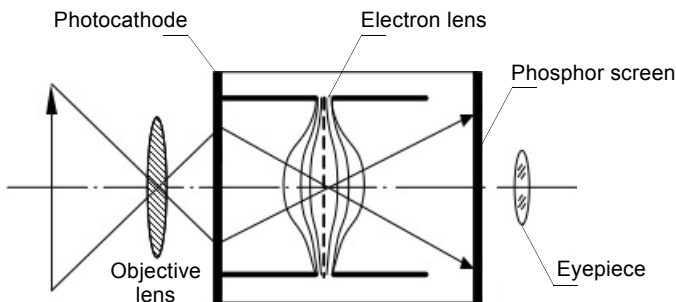


Fig. 1. Structure chart of image intensifier system.

2.2. Quality parameters of image intensifier

In most cases, magnification and distortion are regarded as the quality parameters of image intensifier. The magnification can change the picture size and the distortion can cause anamorphose. Figure 2 shows the representative distortions, they are barrel distortion, pincushion distortion, snake-shaped distortion and shearing distortion, respectively. The barrel distortion or pincushion distortion is called global distortion, the snake-shaped distortion and shearing distortion are called partial distortion.

3. Quality parameters measurement based on projecting phase-shifting gratings

The measuring system is as shown in Fig. 3. While the beam of light from the light source is transformed into collimated light and injected into the spatial light modulator (SLM) to project the phase-shifting gratings, the corresponding deformed patterns modulated

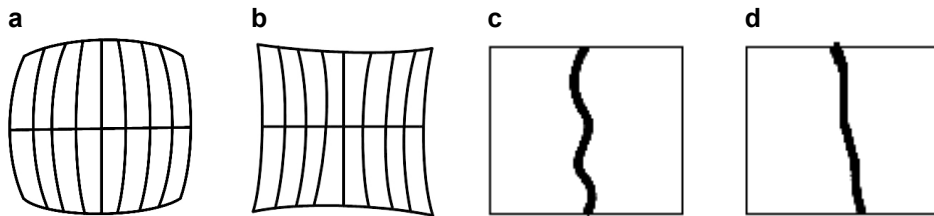


Fig. 2. Barrel (a), pincushion (b), snake-shaped (c), and shearing (d) distortions.

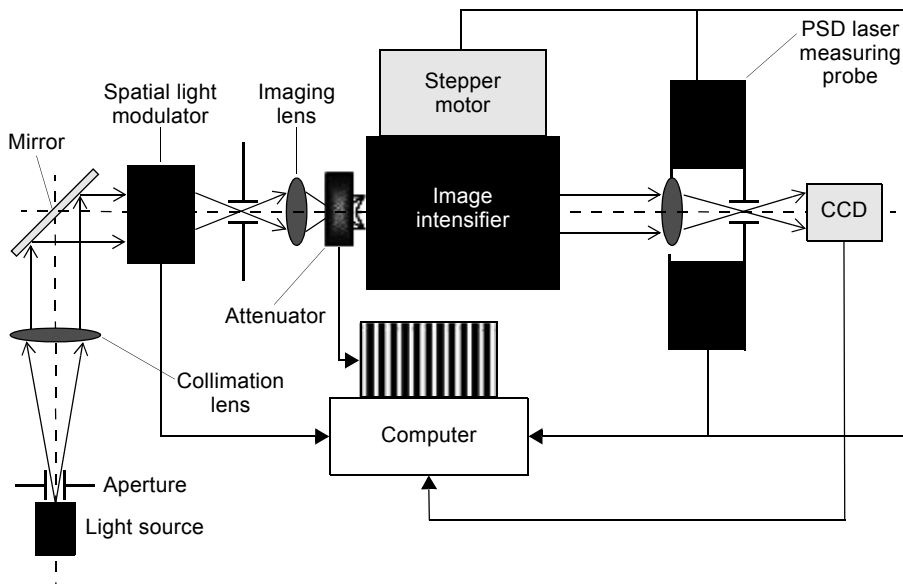


Fig. 3. Schematic of measuring system.

by the measured image intensifier can be captured with the CCD camera. The measuring procedures are composed of the following two parts.

3.1. Preparatory work

Before the image intensifier is measured, the referential grating period needs to be obtained, and the procedures are as follows.

Firstly, a set of phase-shifting gratings are designed, if the background intensity is represented as $B_0(x, y)$, the contrast is represented as $C_0(x, y)$ and the designed grating period is represented as T_0 , then the designed phase-shifting gratings can be expressed as follows:

$$S_0(x, y) = B_0(x, y) + C_0(x, y) \cos\left(\frac{2\pi x}{T_0} + \frac{2\pi n}{5}\right), \quad n = 1, 2, 3, 4, 5 \quad (1)$$

Secondly, the designed phase-shifting gratings are projected into the measuring system orderly by the SLM. Because the measured image intensifier is not installed, the CCD camera can capture the corresponding referential gratings at the same position of the export of the measured image intensifier. If the captured referential grating period is represented as T_1 and the phase introduced by the measuring system is repre-

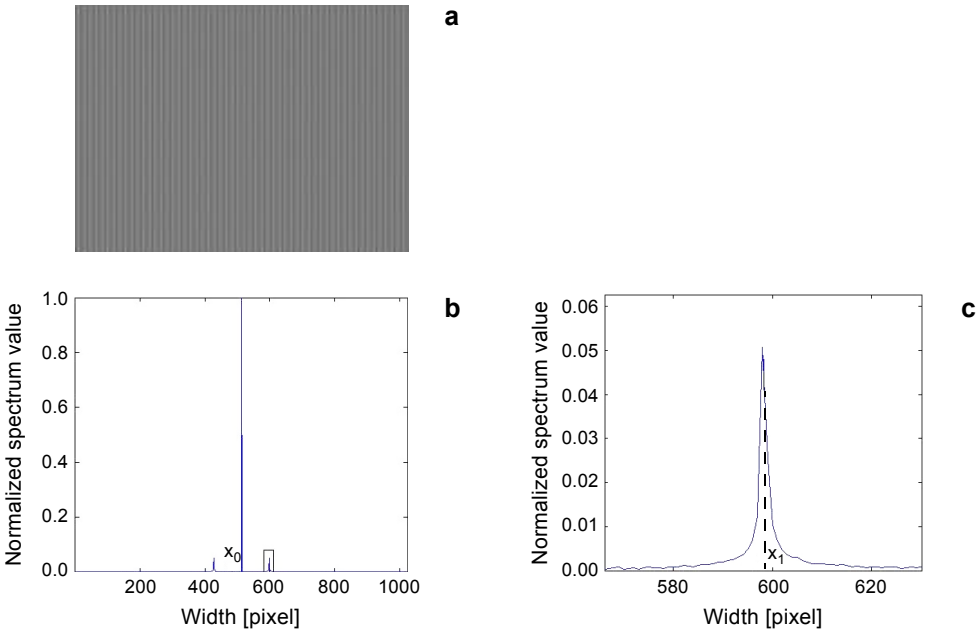


Fig. 4. Processing of captured grating. The captured grating (a). The normalized spectrum of the captured grating a (b). The extracted fundamental frequency from the spectrum b (c).

sented as $\varphi_1(x, y)$, the corresponding captured referential gratings can be expressed as follows:

$$S_1(x, y) = B_1(x, y) + C_1(x, y) \cos\left(\frac{2\pi x}{T_1} + \frac{2\pi n}{5} + \varphi_1(x, y)\right) \quad (2)$$

where (x, y) represents the pixel coordinate of the CCD camera, and $x \in [1, M]$, $y \in [1, N]$, M and N are the width and the height of the image captured with the CCD camera, respectively.

In order to obtain the referential grating period T_1 , the captured referential gratings are processed as follows. As shown in Fig. 4, Fig. 4a is one of the captured referential gratings, Fig. 4b is the normalized spectrum of Fig. 4a obtained by Fourier transform and normalization, the area marked with rectangle is the fundamental frequency component and Fig. 4c is its enlarged view.

Here, the designed grating should satisfy two conditions, one is that the maximum gray value of the grating can be obtained, and the other is that the distribution of gray values at both sides of the maximum gray value is almost symmetric.

As shown in Figs. 4a and 4b, x_0 and x_1 represent the positions of the maximum spectrum values of the background components and the fundamental frequency components, respectively, so the referential grating period can be obtained as follows:

$$T_1 = \frac{M}{x_1 - x_0} \quad (3)$$

3.2. Measuring the quality parameters of image intensifier

Firstly, the measured image intensifier is loaded. While the designed phase-shifting gratings are projected into the measuring system in succession, the corresponding deformed patterns modulated by the measured image intensifier are captured with the CCD camera as follows:

$$S_2(x, y) = B_2(x, y) + C_2(x, y) \cos\left(\frac{2\pi x}{T_2} + \frac{2\pi n}{5} + \varphi_2(x, y)\right) \quad (4)$$

where T_2 represents the magnified grating period by the measured image intensifier, $\varphi_2(x, y)$ represents the phase caused by the measured image intensifier.

The magnified grating period T_2 can be obtained with the method mentioned in Section 3.1, therefore the magnification β of the measured image intensifier can be calculated as follows:

$$\beta = \frac{T_2}{T_1} \quad (5)$$

Secondly, the other set of phase-shifting gratings are designed as follows:

$$S_3(x, y) = B_0(x, y) + C_0(x, y) \cos\left(\frac{2\pi x}{T_3} + \frac{2\pi n}{5}\right) \quad (6)$$

where $T_3 = \beta T_0$.

Thirdly, the measured image intensifier is unloaded. While the new designed phase-shifting gratings are projected into the measuring system in succession, the corresponding gratings at the same position of the export of the measured image intensifier are captured with the CCD camera as follows:

$$S_4(x, y) = B_4(x, y) + C_4(x, y) \cos\left(\frac{2\pi x}{T_4} + \frac{2\pi n}{5} + \varphi_4(x, y)\right) \quad (7)$$

where $\varphi_4(x, y)$ represents the referential phase caused by only the magnification of the measured intensifier.

Phases $\varphi_2(x, y)$ and $\varphi_4(x, y)$ can be calculated as follows:

$$\begin{cases} \varphi_2(x, y) = \operatorname{atan} \left[\frac{\sum_{n=1}^5 S_2(x, y) \sin(2\pi n/5)}{\sum_{n=1}^5 S_2(x, y) \cos(2\pi n/5)} \right] \\ \varphi_4(x, y) = \operatorname{atan} \left[\frac{\sum_{n=1}^5 S_4(x, y) \sin(2\pi n/5)}{\sum_{n=1}^5 S_4(x, y) \cos(2\pi n/5)} \right] \end{cases} \quad (8)$$

Therefore, the phase caused by the distortion of the measured image intensifier can be obtained as follows:

$$\psi(x, y) = \varphi_2(x, y) - \varphi_4(x, y) \quad (9)$$

Because $\varphi_2(x, y)$ and $\varphi_4(x, y)$ come from antitangent calculation, $\psi(x, y)$ is wrapped in $[-\pi, \pi]$. The corresponding continuous phases $\Psi(x, y)$ can be extracted by phase unwrapping [22].

For an image intensifier, the maximum barrel distortion or maximum pincushion distortion may occur at one of the four imaging edges.

Here, D_{left} , D_{right} , D_{top} and D_{bottom} are defined as the distortions at the four edges:

$$D_{\text{left}} = \begin{cases} \frac{\max\{\Psi(1, 1), \Psi(1, N)\} - \min\{\Psi(1, y)\}}{2\pi} T_2 & \text{if disortion is barrel} \\ \frac{\max\{\Psi(1, y)\} - \min\{\Psi(1, 1), \Psi(1, N)\}}{2\pi} T_2 & \text{otherwise} \end{cases} \quad (10)$$

$$D_{\text{right}} = \begin{cases} \frac{\max\{\Psi(M, y)\} - \min\{\Psi(M, 1), \Psi(M, N)\}}{2\pi} T_2 & \text{if disortion is barrel} \\ \frac{\max\{\Psi(M, 1), \Psi(M, N)\} - \min\{\Psi(M, y)\}}{2\pi} T_2 & \text{otherwise} \end{cases} \quad (11)$$

$$D_{\text{top}} = \begin{cases} \frac{\max\{\Psi(1, 1), \Psi(M, 1)\} - \min\{\Psi(x, 1)\}}{2\pi} T_2 & \text{if disortion is barrel} \\ \frac{\max\{\Psi(x, 1)\} - \min\{\Psi(1, 1), \Psi(M, 1)\}}{2\pi} T_2 & \text{otherwise} \end{cases} \quad (12)$$

$$D_{\text{bottom}} = \begin{cases} \frac{\max\{\Psi(x, N)\} - \min\{\Psi(M, 1), \Psi(M, N)\}}{2\pi} T_2 & \text{if disortion is barrel} \\ \frac{\max\{\Psi(1, N), \Psi(M, N)\} - \min\{\Psi(x, N)\}}{2\pi} T_2 & \text{otherwise} \end{cases} \quad (13)$$

Generally, regarding the barrel distortion or pincushion distortion, only one of them can occur, therefore the global distortion of the measured image intensifier is defined as follows:

$$D_z = \max\{D_{\text{left}}, D_{\text{right}}, D_{\text{top}}, D_{\text{bottom}}\} \quad (14)$$

In $\Psi(x, y)$, if a subdomain $\Phi(u, v)$ ($u \in [1, x], v \in [1, y]$) has a phase jump or discontinuous phase, it means that there is the snake-shaped distortion or the shearing distortion. In $\Phi(u, v)$, a phase threshold value is set and then the differences in the phase values in $\Phi(u, v)$ and the phase threshold value are calculated. If the signs of the differences are not consistent, the distortion is the snake-shaped distortion D_{sn} . Otherwise, the distortion is the shearing distortion D_{sh} . The partial distortion is defined as follows:

$$D_b = \frac{\max\{\Phi(u, v)\} - \min\{\Phi(u, v)\}}{2\pi} T_2 \quad (15)$$

4. Computer simulation

In order to satisfy the two conditions mentioned in Section 3.1, the quantity of pixels in half a period of designed grating is an odd number's integral multiple. This means that in ..., $[-2\pi, \pi]$, $[-\pi, 0]$, $[0, \pi]$, $[\pi, 2\pi]$, ... the quantity of pixels of designed grating is an odd number's integral multiple, or else the fidelity of sinusoidal of designed grating could be damaged. For example, when $T_0 = 30$ pixels, "the quantity of pixels in half a period of designed grating is an odd number's integral multiple" can be realized.

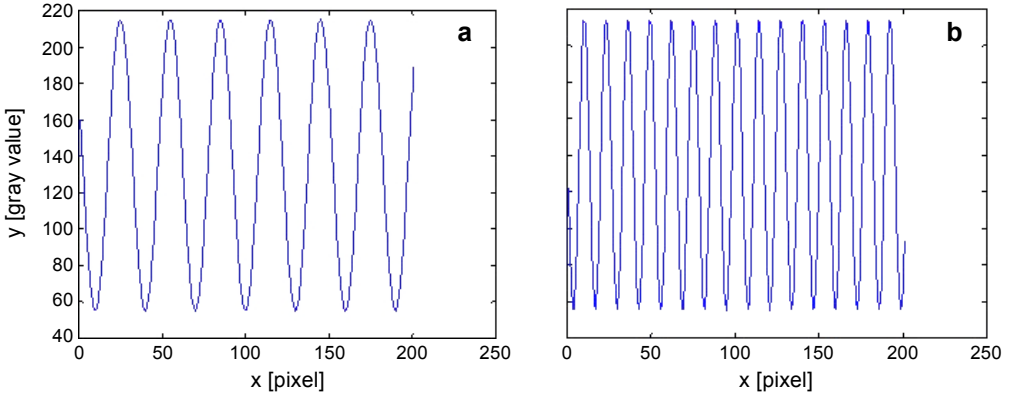


Fig. 5. The fidelity of sinusoid of designed grating. The sinusoid at a line when $T_0 = 30$ pixels (a) and at the same line when $T_0 = 13$ pixels (b).

Figure 5a shows the sinusoid at a line from the designed grating, which is of good fidelity. When $T_0 = 13$ pixels, the constraint condition mentioned above cannot be established, and Fig. 5b shows the sinusoid at the same line from the designed grating, whose fidelity is damaged.

To select a suitable T_0 , the computer simulation is done. A simulated distortion d_c with maximum value 10.00 pixels is constructed. Table 1 shows the statistics result of reconstructed distortion d_{rc} by the proposed method with different T_0 .

Table 1 shows that when T_0 cannot satisfy the condition: “the quantity of pixels in half a period of designed grating is an odd number’s integral multiple” mentioned above, the error between the reconstructed and constructed distortion is high, the corresponding root mean square (RMS) is also high, like at $T_0 = 11$, $T_0 = 17$ or $T_0 = 25$. But when T_0 can satisfy the above condition, like at $T_0 = 10$, $T_0 = 14$, $T_0 = 20$, $T_0 = 24$ or $T_0 = 30$, the error between the reconstructed and constructed distortion is low, and the corresponding RMS is also low. Especially, when $T_0 = 10$, $T_0 = 20$ or $T_0 = 30$, the error is even lower. In the proposed method, the five-step phase shifting method is applied. When $T_0 = 10$, $T_0 = 20$ or $T_0 = 30$, there is no error caused by phase-shifting, and the reconstructed distortion is more accurate.

5. Experiments and analysis

In order to show the performance of the proposed method, thousands of experiments have been performed. Figures 6 and 7 show one of the representative experimental results. The experiment is implemented following the measuring processes described in Section 3. Primarily, the preparatory work is done. Figure 6a shows one of the captured referential gratings and T_1 at this condition can be obtained by the method mentioned in Section 3.1.

The second step: the measured image intensifier is loaded and while the designed phase-shifting gratings are projected into the inport of the measured image intensifier

Table 1. Statistics result of reconstructed distortion.

T_0	d_{rc}	Error	RMS
10	9.91	0.09	0.0021
11	9.41	0.59	0.0852
12	9.88	0.12	0.0053
13	9.53	0.47	0.0627
14	9.89	0.11	0.0081
15	9.59	0.41	0.0607
16	9.83	0.17	0.0079
17	9.32	0.68	0.0867
18	9.85	0.15	0.0049
19	9.46	0.54	0.0921
20	9.93	0.07	0.0019
21	9.50	0.50	0.0578
22	9.80	0.20	0.0032
23	9.60	0.40	0.0577
24	9.87	0.13	0.0063
25	9.39	0.61	0.0759
26	9.78	0.22	0.0053
27	9.48	0.52	0.0721
28	9.86	0.14	0.0069
29	9.51	0.49	0.0827
30	9.92	0.08	0.0013

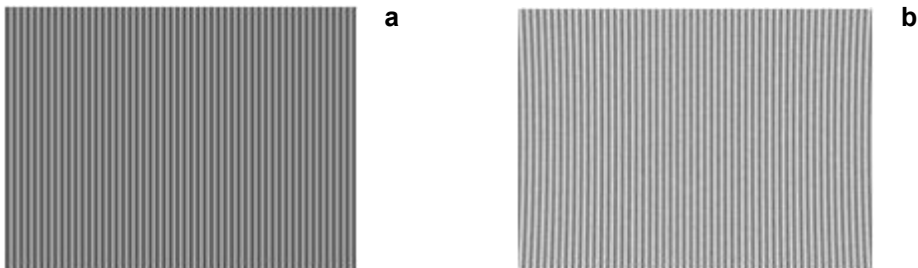


Fig. 6. Captured referential grating (a) and deformed pattern (b).

in succession, the corresponding deformed patterns are captured with the CCD camera. Figure 6b shows one of the captured deformed patterns. T_2 at this condition can be obtained by the same method mentioned in Section 3.1. So β can be calculated according to Eq. (5). In addition, $\varphi_2(x, y)$ can be extracted according to Eq. (8).

The third step: the measured image intensifier is unloaded and while the phase-shifting gratings designed according to Eq. (6) are projected into the measuring system orderly, the corresponding gratings at the same position of the export of the measured image intensifier are captured with the CCD camera, and $\varphi_4(x, y)$ can be extracted ac-

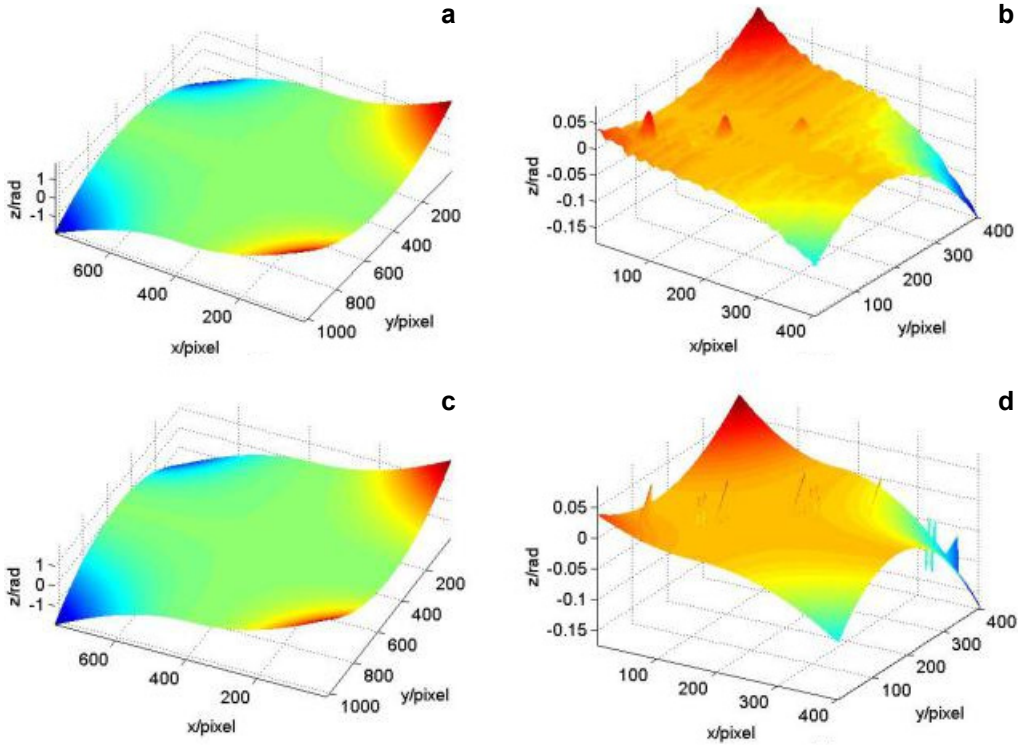


Fig. 7. Retrieved phase caused by the global distortion of the image intensifier by FTPM (a). The phase distribution caused by partial distortion extracted from image a (b). Retrieved phase caused by the global distortion of the image intensifier by PPSG (c). The phase distribution caused by partial distortion extracted from image c (d).

according to Eq. (8). The phase caused by the distortion of the measured image intensifier can be obtained according to both Eq. (9) and phase unwrapping.

Here, FTPM is used to do a comparison with PPSG. The comparative experimental results are shown as Fig. 7.

Figure 7a is the retrieved phase caused by the global distortion of the measured image intensifier with FTPM, and Fig. 7b is the phase caused by the partial distortion of the measured image intensifier extracted from Fig. 7a. Figure 7c is the phase caused by the global distortion of the measured image intensifier with PPSG, and Fig. 7d is the phase caused by the partial distortion of the measured image intensifier extracted from Fig. 7c.

As we can see, Fig. 7a seems to be the same as Fig. 7c. But actually it is not so, because the filtering operation in the frequency domain may definitely lead to spatial information losses at every position as a whole. But the point-to-point phase calculation from more than three frames phase-shifting deformed patterns without any filtering operation in PPSG can guarantee the spatial information integrity at every position.

Table 2. Statistics of measuring results.

Selected methods	Magnification		Distortion [pixel]					
	$\bar{\beta}$	RMS_{β}	\bar{D}_z	RMS_{D_z}	\bar{D}_{sn}	$\text{RMS}_{D_{\text{sn}}}$	\bar{D}_{sh}	$\text{RMS}_{D_{\text{sh}}}$
FTPM	1.09	0.014	8.13	0.098	0.57	0.065	1.18	0.070
Proposed	1.10	0.006	8.22	0.063	1.25	0.012	2.33	0.016

So, the fidelity of PPSG is higher than that of FTPM. This evidence can also be revealed by comparing Fig. 7b and Fig. 7d. The partial distortion, including snake-shaped distortion and shearing distortion, show the quick image distortion in a small local range and reflect abundant high-frequency information. Due to the filtering operation, the sharp peaks in Fig. 7b are smoothed and the gentle zones in Fig. 7b are wrinkled. It reveals that the high frequency components of the partial distortion have been lost. On the contrary, both the sharp peaks and the gentle zones in Fig. 7d retain their true features. It reveals that the fidelity of the partial distortion can be guaranteed in the proposed PPSG method.

The comparative experimental results show that the obtained phase caused by the distortions of the measured image intensifier can reveal their true features more effectively with PPSG.

The distortion of the measured image intensifier can be calculated by the phase-to-distortion matching according to Eqs. (10)–(15). We have measured the same image intensifier for ten times. Its statistics of measuring results are shown in Table 2.

The statistics shows that both FTPM and PPSG can measure the multiple quality parameters of image intensifier, including the magnification, global distortion, snake-shaped distortion and shearing distortion. No matter which parameter is measured, the corresponding RMS with PPSG is always smaller than that with FTPM, which means that the measuring repeatability of PPSG is better than that of FTPM, especially in the partial distortion measurement.

In summary, the experimental results show that the proposed method can effectively measure the multiple quality parameters of image intensifier, including the magnification, global distortion, snake-shaped distortion and shearing distortion with higher accuracy and higher repeatability.

6. Conclusion

A method for measuring the quality parameters of image intensifier based on projecting phase-shifting gratings is proposed. The designed phase-shifting gratings are respectively projected into the measuring system in order to obtain the magnification parameter of the measured image intensifier, and the referential phase caused by only the magnification of the measured image intensifier. The phase caused by the distortion of the measured image intensifier is obtained by phase unwrapping. The distortions of the measured image intensifier are measured by the phase-to-distortion matching suc-

cessfully. The experimental results show that the proposed method can effectively measure the multiple quality parameters of image intensifier, including the magnification, global distortion, snake-shaped distortion and shearing distortion.

Acknowledgments – The work was supported by PRC National Plan Foundation (2007AA01Z333) and PRC Special National Project (2009ZX02204-008).

References

- [1] IMAMURA Y., OKI E., OHGAKI K., NAKASHIMA Y., ANDO K., TSUTSUMI S., TSURUMARU D., SAEKI H., BABA H., MAEHARA Y., *Real-time accurate identification of tumor site using a mobile X-ray image-intensifier system during laparoscopic gastrectomy*, [Journal of the American College of Surgeons 222\(2\), 2016, pp. E1–E7.](#)
- [2] YUANHE TANG, YANG YU, HAIYANG GAO, SHULIN LIU, XIAOLIN WANG, *Study on magnetic mirror array image intensifier to work at room temperature*, [Applied Optics 54\(26\), 2015, pp. 8010–8017.](#)
- [3] YAGI N., AOYAMA K., *An X-ray image intensifier for microsecond time-resolved experiments*, [Journal of Instrumentation 10, 2015, article ID T01002.](#)
- [4] SHENGTAO YU, XULEI QIN, YE LI, *The method of X-ray image intensifies pixel matching and noise suppression based on the CCD*, [Proceedings of SPIE 10141, 2016, article ID 101411C.](#)
- [5] XIA WANG, WEIQI JIN, ZHIYUN GAO, ZHIHONG WANG, TINGZHU BAI, *Research on digitally integrated test system for performance evaluation of image intensifier and intensified CCD*, [Proceedings of SPIE 6150, 2006, article ID 61500S.](#)
- [6] McDONALD T.E., YATES G.J., KING N.S.P., TURKO B.T., *Continuous-recording camera system for high-frame-rate high-resolution applications*, [Proceedings of SPIE 3516, 1999, pp. 322–331.](#)
- [7] YANHONG LI, XIAOMEI CHEN, GUOQIANG NI, *Application research on microchannel plate in new fields*, [Proceedings of SPIE 9620, 2015, article ID 96200W.](#)
- [8] QIUCHENG SUN, YUEQIAN HOU, JIAN CHEN, *Lens distortion correction for improving measurement accuracy of digital image correlation*, [Optik – International Journal for Light and Electron Optics 126\(21\), 2015, pp. 3153–3157.](#)
- [9] KEDGLEY A.E., FOX A.-M.V., JENKYN T.R., *Image intensifier distortion correction for fluoroscopic RSA: the need for independent accuracy assessment*, [Journal of Applied Clinical Medical Physics 13\(1\), 2012, pp. 197–204.](#)
- [10] McROBBIE D.W., NIETO-CAMERO J.J., *Measurement of image intensifier system modulation transfer function by video signal analysis*, [Medical Physics 21\(2\), 1994, pp. 257–264.](#)
- [11] CUELENAERE A.J., *Critical parameters in the photometric measurements of image intensifier tubes*, [Proceedings of SPIE 73, 1976, pp. 66–70.](#)
- [12] SONG SUN, YIPING CAO, TAO CHEN, XIYU ZENG, *Multi-parameter measuring method of image intensifier based on Fourier transform phase measurement*, [Optik – International Journal for Light and Electron Optics 125\(15\), 2014, pp. 4168–4171.](#)
- [13] FENG LUO, WENJING CHEN, XIANYU SU, *Eliminating zero spectra in Fourier transform profilometry by application of Hilbert transform*, [Optics Communications 365, 2016, pp. 76–85.](#)
- [14] SENPENG CAO, YIPING CAO, QICAN ZHANG, *Fourier transform profilometry of a single-field fringe for dynamic objects using an interlaced scanning camera*, [Optics Communications 367, 2016, pp. 130–136.](#)
- [15] TONGCHUAN LIU, CANLIN ZHOU, YEPENG LIU, SHUCHUN SI, ZHENKUN LEI, *Deflectometry for phase retrieval using a composite fringe*, [Optica Applicata 44\(3\), 2014, pp. 451–461.](#)
- [16] JOENATHAN C., BERNAL A., YOUN WOONGHEE, YANZENG LI, WANSEOK OH, *Analysis of the quantitative measurement for a lateral shear interferometer in a convergent beam mode using Fourier transform method*, [Optical Engineering 53\(5\), 2014, article ID 054109.](#)
- [17] SRINIVASAN V., LIU H.C., HALIOUA M., *Automated phase-measuring profilometry of 3-D diffuse objects*, [Applied Optics 23\(18\), 1984, pp. 3105–3108.](#)

- [18] ZHUANG MAO, YIPING CAO, LIJUN ZHONG, SENPENG CAO, *A method for improving the precision of on-line phase measurement profilometry*, [Optica Applicata 45\(1\), 2015, pp. 51–61.](#)
- [19] ZHENFEN HUANG, YIPING CAO, AIPING ZHAI, YANG LI, DELIANG CHEN, *Active phase-setting twin-frequency grating for 3D shape measurement based on an absolute phase unwrapping algorithm*, [Optica Applicata 42\(4\), 2012, pp. 887–900.](#)
- [20] YUANKUN LIU, QICAN ZHANG, XIANYU SU, *3D shape from phase errors by using binary fringe with multi-step phase-shift technique*, [Optics and Lasers in Engineering 74, 2015, pp. 22–27.](#)
- [21] PENG WANG, YIPING CAO, XIN YANG, KUANG PENG, *On-line phase measuring profilometry for a rotating object*, [Optical Engineering 53\(11\), 2014, article ID 114112.](#)
- [22] XIANYU SU, QICAN ZHANG, *Phase unwrapping in the dynamic 3D measurement*, [AIP Conference Proceedings 1236\(1\), 2010, pp. 467–471.](#)

*Received January 14, 2017
in revised form April 24, 2017*